

# Spin-orbital Entangled Molecular $j_{\text{eff}}$ States in Lacunar Spinel Compounds

Heung-Sik Kim,<sup>1</sup> Jino Im,<sup>2</sup> Myung Joon Han,<sup>1,3</sup> and Hosub Jin<sup>4,5,\*</sup>

<sup>1</sup>*Department of Physics, Korean Advanced Institute  
of Science and Technology, Daejeon 305-701, Korea*

<sup>2</sup>*Department of Physics and Astronomy,  
Northwestern University, Evanston, Illinois 60208, USA*

<sup>3</sup>*KAIST Institute for the NanoCentury,  
Korean Advanced Institute of Science and Technology, Daejeon 305-701, Korea*

<sup>4</sup>*Center for Correlated Electron Systems,  
Institute for Basic Science (IBS), Seoul 151-747, Korea*

<sup>5</sup>*Department of Physics and Astronomy,  
Seoul National University, Seoul 151-747, Korea*

The entanglement of the spin and orbital degrees of freedom through the spin-orbit coupling has been actively studied in condensed matter physics. In several iridium-oxide systems, the spin-orbital entangled state, identified by the effective angular momentum  $j_{\text{eff}}$ , can host novel quantum phases with the help of electron correlations. Here we show that a series of lacunar spinel compounds,  $\text{Ga}M_4X_8$  ( $M = \text{Nb, Mo, Ta, and W}$  and  $X = \text{S, Se, and Te}$ ), gives rise to a molecular  $j_{\text{eff}}$  state as a new spin-orbital composite on which the low energy effective Hamiltonian is based. A wide range of electron correlations is accessible by tuning the bandwidth under external and/or chemical pressure, enabling us to investigate the interesting cooperation between spin-orbit coupling and electron correlations. As illustrative examples, a two-dimensional topological insulating phase and an anisotropic spin Hamiltonian are investigated in the weak and strong coupling regimes, respectively. Our finding can provide an ideal platform for exploring  $j_{\text{eff}}$  physics and the resulting emergent phenomena.

Spin-orbit coupling (SOC) is a manifestation of Einstein's theory of relativity in condensed matter systems. Recently, SOC has attracted a great deal of attention since it is a main ingredient for spintronics applications<sup>1,2</sup>, induces novel quantum phases<sup>3,4</sup>, and generates new particles and elementary excitations<sup>5,6</sup>. Moreover, when incorporated with electron correlations, SOC can give rise to even more fascinating phenomena<sup>7,8</sup>. In the iridium oxide family, where the  $\text{IrO}_6$  octahedron is the essential building block, various quantum phases have been predicted or verified according to the electron correlation strength on top of the large SOC of the Ir  $5d$   $t_{2g}$  orbital: topological band insulator for weak coupling<sup>9,10</sup>, Weyl semi-metal, axion insulator, non-Fermi liquid, and  $\text{TI}^*$  phases for intermediate coupling<sup>11-15</sup>, and topological Mott insulator and quantum spin liquid phases for strong coupling<sup>7,16,17</sup>.

Emergence of the spin-orbital entangled  $j_{\text{eff}}$  states induced by SOC<sup>18,19</sup> is the key feature to host all the above phases, yet the existence of such states is limited to a small number of iridate compounds only. Here, the series of lacunar spinel compounds<sup>20,21</sup>,  $\text{Ga}M_4X_8$ , where early  $4d$  or  $5d$  transition metal atoms occupy the  $M$ -site, are found to provide the molecular form of the  $j_{\text{eff}}$  basis in their low energy electronic structures. The idealness of the molecular  $j_{\text{eff}}$  state is guaranteed by the formation of the  $M_4$  metal cluster and the large SOC. Combined with the ability to control the electron correlation from the weak to strong coupling limit, the lacunar spinels can manifest themselves as the best candidates to

demonstrate this so-called  $j_{\text{eff}}$  physics.

## Results

**Formation of the molecular  $j_{\text{eff}}$  states in  $\text{GaTa}_4\text{Se}_8$ .** The chemical formula and crystal structure of the  $\text{Ga}M_4X_8$  lacunar spinels are easily deduced from the spinel with half-deficient Ga atoms, *i.e.*  $\text{Ga}_{0.5}M_2X_4$ . Due to the half-removal of the Ga atoms, the transition metal atoms are strongly distorted into the tetrahedral center as denoted by the red arrows in Fig. 1 **a**, and a tetramerized  $M_4$  cluster appears. The  $M_4$  cluster yields a short intra-cluster  $M$ - $M$  distance, naturally inducing the molecular states residing on the cluster as basic building blocks for the low energy electronic structure. On the other hand, the large inter-cluster distance results in a weak inter-cluster bonding and a narrow bandwidth of the molecular states.

As a representative example of the lacunar spinels, we investigate the electronic structure of  $\text{GaTa}_4\text{Se}_8$  (Fig. 1 **b-d**). Figure 1 **b** shows the band structure and the projected density of states (PDOS) of  $\text{GaTa}_4\text{Se}_8$  in the absence of SOC. In consistency with previous studies<sup>21–23</sup>, the triply degenerate molecular  $t_2$  bands occupied by one electron are located near the Fermi level with a small bandwidth of  $\sim 0.75$  eV. (See Supplementary Note 1, Supplementary Figure 1, and Supplementary Table 1 for details on the molecular  $t_2$  effective Hamiltonian.) As shown in the PDOS plot, the molecular  $t_2$  bands are dominated by Ta  $t_{2g}$  orbital components; the small admixture of Se  $5p$  and the strong tetramerization imply that the molecular  $t_2$  states consist of direct bonding between Ta  $t_{2g}$  states.

The molecular nature of the low-energy electronic structure can be visualized by adopting the maximally localized Wannier function scheme<sup>24,25</sup>. The three molecular  $t_2$  Wannier functions depicted in Fig. 1 **c** read

$$|D_\alpha\rangle = \frac{1}{2} \sum_{i=1}^4 |d_\alpha^i\rangle \quad (\alpha = xy, yz, zx), \quad (1)$$

where  $D_\alpha$  and  $d_\alpha$  denote the molecular  $t_2$  and atomic  $t_{2g}$  states, respectively, and  $i$  is a site index indicating the four corners of the  $M_4$  cluster. Each  $D_\alpha$  originates from a  $\sigma$ -type strong bonding between the constituent  $t_{2g}$  orbitals in the  $M_4$  cluster. Owing to the exact correspondence between the molecular  $t_2$  and the atomic  $t_{2g}$  states, as revealed in Eq. 1, the molecular  $t_2$  triplet carries the same effective orbital angular momentum  $l_{\text{eff}} = 1$  as the atomic  $t_{2g}$  orbital<sup>18</sup>. By virtue of SOC, the  $l_{\text{eff}} = 1$  states are entangled with the  $s$

= 1/2 spin, and two multiplets designated by the effective total angular momentum  $j_{\text{eff}} = 1/2$  and  $3/2$  emerge. The band structure and PDOS of  $\text{GaTa}_4\text{Se}_8$  in the presence of SOC verify the above  $j_{\text{eff}}$  picture (Fig. 1 **d**); the molecular  $t_2$  bands split into upper  $j_{\text{eff}} = 1/2$  and lower  $j_{\text{eff}} = 3/2$  bands. The separation between the two  $j_{\text{eff}}$  subbands is almost perfect owing to the large SOC of the Ta atoms as well as the small bandwidth of the molecular  $t_2$  band. An alternative confirmation of the  $j_{\text{eff}}$  picture can also be given by constructing the Wannier function from each of the  $j_{\text{eff}}$  subbands, which shows a 99% agreement with the ideal molecular  $j_{\text{eff}}$  states. (See Supplementary Figure 2.) Consequently, the electronic structure of  $\text{GaTa}_4\text{Se}_8$  can be labeled as a quarter-filled  $j_{\text{eff}} = 3/2$  system on a face-centered cubic lattice.

**Robust  $j_{\text{eff}}$ -ness in the  $\text{Ga}M_4X_8$  series.** The aforementioned  $j_{\text{eff}}$ -ness in  $\text{GaTa}_4\text{Se}_8$  remains robust in the  $\text{Ga}M_4X_8$  series with a neighboring  $5d$  transition metal ( $M = \text{W}$ ) as well as the  $4d$  counterparts ( $M = \text{Nb}$  and  $\text{Mo}$ ). Among the series,  $M = \text{W}$  compounds have not been reported previously in experiments. Thus we use optimized lattice parameters by structural relaxations. In Fig. 2 **a-d**, the electronic structures of  $\text{GaTa}_4\text{Se}_4\text{Te}_4$ <sup>26</sup>,  $\text{GaW}_4\text{Se}_4\text{Te}_4$ ,  $\text{GaNb}_4\text{Se}_8$ <sup>21</sup>, and  $\text{GaMo}_4\text{Se}_8$ <sup>27</sup> are shown – band structure, PDOS, and Fermi surface with projection onto the molecular  $j_{\text{eff}}$  states. In Fig. 2 **a** and **b**, one can see the clear separation and identification of the higher  $j_{\text{eff}} = 1/2$  doublet and the lower  $j_{\text{eff}} = 3/2$  quartet driven by the large SOC of the  $5d$  transition metal atoms. The overall band dispersions are quite similar except for the location of the Fermi level; the  $M = \text{Ta}$  and  $M = \text{W}$  lacunar spinels are well characterized by the quarter-filled  $j_{\text{eff}} = 3/2$  and the half-filled  $j_{\text{eff}} = 1/2$  systems, respectively. In  $4d$  compounds, the separation between the  $j_{\text{eff}}$  subbands is reduced due to the smaller SOC compared with the  $5d$  systems (Fig. 2 **c** and **d**). Nevertheless, there is a discernible splitting between the  $j_{\text{eff}} = 1/2$  and  $3/2$  bands, which is comparable to or even better than that in the prototype  $j_{\text{eff}}$  compounds,  $\text{Sr}_2\text{IrO}_4$  and  $\text{Ba}_2\text{IrO}_4$ <sup>28</sup>.

To acquire a well-identified  $j_{\text{eff}}$  band, we need the  $j_{\text{eff}}$  state as a local basis, and the inter-orbital hopping terms between the  $j_{\text{eff}}$  subspaces should be suppressed. Hence, there are three important conditions to realize the ideal  $j_{\text{eff}}$  system: high symmetry protecting the  $l_{\text{eff}}=1$  three-fold orbital degeneracy, small bandwidth minimizing the inter-orbital mixing, and large SOC fully entangling the spin and orbital degrees of freedom. The lacunar spinel compounds comfortably satisfy the above conditions; the tetrahedral symmetry of the  $M_4$  cluster protects the orbital degeneracy, the long inter-cluster distance leads to the small

bandwidth, and a large SOC is inherent in  $4d$  and  $5d$  transition metal atoms.

Figure 2 e introduces one important controlling parameter – the bandwidth. By changing the inter-cluster distance via external pressure and/or by substituting chalcogen atoms, the bandwidth of the molecular  $t_2$  band can be tuned over a wide range. In the  $M = \text{Ta}$  series, for example, the bandwidth varies from 0.4 to 1.1 eV. Consequently, the effective electron correlation strength, given by the ratio between the bandwidth and the on-site Coulomb interactions, can be controlled to reach from the weak to the strong coupling regime. In fact, the bandwidth-controlled insulator-to-metal transitions were observed in  $\text{GaTa}_4\text{Se}_4$  and  $\text{GaNb}_4\text{Se}_4$ <sup>23,29</sup>, implying that both the weakly and strongly interacting limits are accessible in a single compound.

**Effective Hamiltonian.** From the apparent separation between the  $j_{\text{eff}}$  subbands, as well as the similar band dispersions, the  $\text{Ga}M_4X_8$  series are governed by a common effective Hamiltonian composed of two independent  $j_{\text{eff}} = 1/2$  and  $3/2$  subspaces, *i.e.*  $\mathcal{H}_{\text{eff}} \simeq \mathcal{H}^{1/2} \oplus \mathcal{H}^{3/2}$ . (See Supplementary Note 2 and 3.) Therefore, the compounds with  $M = \text{Nb/Ta}$  and  $M = \text{Mo/W}$  are described by the quarter-filled  $\mathcal{H}^{3/2}$  and the half-filled  $\mathcal{H}^{1/2}$  systems, respectively. The nearest-neighbor hopping terms for each subspace are written as

$$\mathcal{H}_{\text{hopping}}^\tau = \sum_{\langle ij \rangle} \mathbf{C}_{i\tau}^\dagger \mathbf{T}_{ij}^\tau \mathbf{C}_{j\tau} \quad (\tau = 1/2, 3/2), \quad (2)$$

with  $\mathbf{T}_{ij}^{1/2} = t^0 \mathbf{I} + it_{ij}^{\text{D}} \cdot \mathbf{S}^{1/2}$

$$\mathbf{T}_{ij}^{3/2} = t^0 \mathbf{I} + it_{ij}^{\text{D}} \cdot \mathbf{S}^{3/2} + \mathbf{t}_{ij}^{\text{Q}} \cdot \mathbf{\Gamma},$$

where  $\mathbf{S}^{1/2}$  and  $\mathbf{S}^{3/2}$  are the  $j_{\text{eff}} = 1/2$  and  $3/2$  pseudospin matrices, respectively, and  $\mathbf{\Gamma}$  are the 5-component Dirac Gamma matrices.  $t^0$  and  $\mathbf{t}^{\text{Q}}$ 's are even, and  $\mathbf{t}^{\text{D}}$ 's are odd functions under the spatial inversion;  $\mathbf{t}^{\text{D}}$ 's are allowed by the inversion asymmetry of the  $M_4$  cluster. The pseudospin-dependent hopping terms  $\mathbf{t}^{\text{D}}$  and  $\mathbf{t}^{\text{Q}}$  can be interpreted as the effective magnetic dipolar and quadrupolar fields acting on the hopping electron, respectively.

**DFT+SOC+ $U$  calculations.** So far, we have discussed about the  $j_{\text{eff}}$ -ness without containing electron correlations, which provides a valid picture in the weak coupling regime. Once taking electron correlations into account, one important question arises on the robustness of the molecular  $j_{\text{eff}}$  states under the influence of the on-site Coulomb interaction. To answer this question, we perform DFT+SOC+ $U$  calculations for  $\text{GaTa}_4\text{Se}_4\text{Te}_4$ ,  $\text{GaW}_4\text{Se}_4\text{Te}_4$ ,  $\text{GaNb}_4\text{Se}_8$ , and  $\text{GaMo}_4\text{Se}_8$ . We consider two simplest magnetic configura-

tions, ferromagnetic and antiferromagnetic order, and the antiferromagnetic solutions for each compound are shown in Fig. 3. In the  $5d$  compounds, the molecular  $j_{\text{eff}}$  states remain robust with developing a SOC-assisted Mott gap within each  $j_{\text{eff}}$  subspace (Fig. 3 **a** and **b**). For the  $4d$  compounds, the  $j_{\text{eff}}$  character is enhanced from the non-interacting cases in Fig. 2 **c** and **d**; the occupied states in  $\text{GaNb}_4\text{Se}_8$  (Fig. 3 **c**) and the unoccupied states in  $\text{GaMo}_4\text{Se}_8$  (Fig. 3 **d**) are dominated by  $j_{\text{eff}}=3/2$  and  $1/2$  characters, respectively. The strengthened  $j_{\text{eff}}$  character by the cooperation with electron correlations is consistent with the recent theoretical results on  $\text{Sr}_2\text{IrO}_4$ <sup>28,30</sup>. See the Supplementary Note 4, Supplementary Figure 3-6, and Supplementary Table 2-5 for more details.

## Discussion

The effective Hamiltonian of the lacunar spinel series has intriguing implications both in the weak and strong coupling regimes. As suggested in previous studies<sup>3,9,31</sup>, the effective fields exerted on the hopping electron can induce a topological insulating phase in the weak coupling regime. In fact, a non-trivial band topology is realized within the molecular  $j_{\text{eff}}$  bands in thin film geometries: the monolayer (Fig. 4 **a**) and the bilayer thin film (Fig. 4 **b**) of the  $M_4$  clusters normal to the (111)-direction. Each system corresponds to the triangular and honeycomb lattice, respectively, and the inter-layer coupling enhanced by a factor of three is adopted in the bilayer system. Non-trivial gaps emerge in the half-filled  $j_{\text{eff}} = 3/2$  bands in the monolayer and the half-filled  $j_{\text{eff}} = 1/2$  bands in the bilayer system. A two-dimensional topological insulator phase is indicated by an odd number of edge Dirac cones at time-reversal invariant momenta in ribbon geometries (Fig. 4 **a** and **b**). Such two-dimensional geometries might be feasible with the help of the state-of-the-art epitaxial technique prevailing in oxide perovskite compounds<sup>32</sup>, or by mechanically cleaving the single crystal to get clean surfaces as done in previous studies on  $\text{GaTa}_4\text{Se}_8$ <sup>33,34</sup>.

In the strong coupling regime, the large on-site Coulomb terms are added to the kinetic Hamiltonian, and the hopping terms  $\mathbf{T}_{ij}^\tau$  are treated as perturbations. The localized  $j_{\text{eff}}$  pseudospins become low-energy degrees of freedom and exchange interactions between the neighboring  $j_{\text{eff}}$  moments emerge. In the simplest example, the one-band Hubbard model within the half-filled  $\mathcal{H}^{1/2}$ , the resulting spin Hamiltonian for the  $j_{\text{eff}} = 1/2$  moments is written as<sup>35,36</sup>

$$\mathcal{H}_{\text{spin}}^{1/2} = \sum_{\langle ij \rangle} [\mathbf{J}\mathbf{s}_i \cdot \mathbf{s}_j + \mathbf{D}_{ij} \cdot (\mathbf{s}_i \times \mathbf{s}_j) + \mathbf{s}_i \cdot \mathbf{A}_{ij} \cdot \mathbf{s}_j], \quad (3)$$

Among the exchange interaction terms, the Dzyaloshinskii-Moriya  $\mathbf{D}_{ij}$  and the pseudodipolar interaction  $\mathbf{A}_{ij}$  depend on  $\mathbf{t}_{ij}^D$ , whose direction is determined by the two mirror planes, as illustrated in Fig. 4 **c** (details in Supplementary Note 5). As shown in Fig. 4 **d**, the relative magnitude of each exchange term is changed with different chalcogen atoms, so that systematic study of the anisotropic Hamiltonian in Eq. 3 can be made in the  $M = \text{Mo/W}$  compounds. Especially,  $\text{GaMo}_4\text{S}_8$  and  $\text{GaW}_4\text{Se}_8$  satisfies the limit of  $|t^0/t^D| \rightarrow 0$ , where the spin Hamiltonian becomes highly anisotropic and bond-direction-dependent such that

$$\begin{aligned} \mathcal{H}_{\text{spin}}^{1/2} &\rightarrow \sum_{\langle ij \rangle} \mathbf{s}_i \cdot \mathbf{A}_{ij} \cdot \mathbf{s}_j \\ &= \frac{4|\mathbf{t}^D|^2}{U} \sum_{\langle ij \rangle} \left[ 2(\mathbf{s}_i \cdot \hat{\mathbf{t}}_{ij}^D)(\mathbf{s}_j \cdot \hat{\mathbf{t}}_{ij}^D) - \mathbf{s}_i \cdot \mathbf{s}_j \right], \end{aligned} \quad (4)$$

with  $\hat{\mathbf{t}}_{ij}^D = \mathbf{t}_{ij}^D/|\mathbf{t}^D|$ . In addition to the Heisenberg term, the Hamiltonian contains the bond-dependent and Ising-like pseudodipolar interaction, called as a Heisenberg-compass model<sup>37</sup>. It can be further reduced to distinct two-dimensional spin models in thin film geometries. Figures 4 **e** and **f** show two examples — the (001)- and (111)-monolayer lead to the 90°- and 60°-compass model with the Heisenberg exchange term on a square and a triangular lattice, respectively.

The  $j_{\text{eff}}=3/2$  systems in the strong coupling limit could also have a significant implication in terms of unconventional multipolar orders<sup>38–40</sup>. On top of the nonmagnetic insulating behavior, the weak tetragonal superstructure and the anomalous magnetic response observed in  $\text{GaNb}_4\text{S}_8$  at  $T \sim 31 \text{ K}$ <sup>41</sup> could give some clues on the quadrupolar ordered phase as well as the spin liquid phase suggested in Ref. 39, which promptly calls for further research on the  $j_{\text{eff}}=3/2$  spin model.

The formation of the  $M_4$  cluster and SOC are the essential requisites to realize the molecular  $j_{\text{eff}}$  state in these three-dimensional intermetallic compounds. The strong tetramerization sustains the isolated molecular bands with three-fold orbital degeneracy and narrow bandwidth, and the large SOC fully entangles the spin and orbital components. The existence of the pure quantum state has been shedding light on studying the ideal quantum model systems in strongly correlated physics; the Hubbard Hamiltonian or the frustrated spin Hamiltonian based on the pure spin-half state have been realized in several organic compounds<sup>42–44</sup>. Likewise, the molecular form of the ideal  $j_{\text{eff}}$  state as a pure quantum

state might be of great use to explore the emergent phenomena in the spin-orbit coupled correlated electron systems.

## Methods

**First-principles calculations** Structural optimizations were done with the projector augmented wave potentials and the PBEsol<sup>45</sup> generalized gradient approximation as implemented in the Vienna *ab-initio* Simulation Package<sup>46,47</sup>. Momentum space integrations were performed on a  $12 \times 12 \times 12$  Monkhorst-Pack grid, and a 300 eV energy cutoff was used for the plane-wave basis set. The force criterion was  $10^{-3}$  eV/Å, and the pressures exerted were estimated by using the Birch-Murnaghan fit.

For the electronic structure calculations, we used OPENMX code<sup>48</sup> based on the linear-combination-of-pseudo-atomic-orbital basis formalism. 400 Ry of energy cutoff was used for the real-space integration. SOC was treated via a fully relativistic  $j$ -dependent pseudo potential in a non-collinear scheme. Simplified DFT+ $U$  formalism by Dudarev *et al.*<sup>49</sup>, implemented in OPENMX code<sup>50</sup>, was adopted in the DFT+SOC+ $U$  calculations.  $U_{\text{eff}} \equiv U - J = 2.5$  and 2.0 eV was used for the  $4d$  and  $5d$  compounds, respectively.

**Acknowledgments** We thank Yong-Baek Kim, Eun-Gook Moon, Tae-Won Noh, and Je-Geun Park for helpful discussions. This work was supported by the Institute for Basic Science (IBS) in Korea. Computational resources were provided by the National Institute of Supercomputing and Networking/Korea Institute of Science and Technology Information with supercomputing resources including technical support (Grant No. KSC-2013-C2-005).

**Competing financial interests** The authors declare no competing financial interests.

---

\* Correspondence: jinhs76@snu.ac.kr

<sup>1</sup> Datta, S. & Das, B. Electronic analog of the eletro-optic modulator. *Applied Physics Letters* **56**, 665 (1990).

<sup>2</sup> Pesin, D. & MacDonald, A. H. Spintronics and pseudospintronics in graphene and topological insulators. *Nature Materials* **11**, 409–416 (2012).

<sup>3</sup> Kane, C. L. & Mele, E. J. Quantum Spin Hall Effect in Graphene. *Physical Review Letters* **95**, 226801 (2005).

<sup>4</sup> Chang, C.-Z. *et al.* Experimental Observation of the Quantum Anomalous Hall Effect in a



- Magnetic Topological Insulator. *Science* **340**, 167–170 (2013).
- <sup>5</sup> Qi, X.-L., Li, R., Zang, J. & Zhang, S.-C. Inducing a magnetic monopole with topological surface states. *Science* **323**, 1184–1187 (2009).
- <sup>6</sup> Fu, L. & Kane, C. L. Superconducting proximity effect and Majorana fermions at the surface of a topological insulator. *Physical Review Letters* **100**, 096407 (2008).
- <sup>7</sup> Pesin, D. & Balents, L. Mott physics and band topology in materials with strong spin-orbit interaction. *Nature Physics* **6**, 376–381 (2010).
- <sup>8</sup> Witczak-Krempa, W., Chen, G., Kim, Y. B. & Balents, L. Correlated Quantum Phenomena in the Strong Spin-Orbit Regime. *Annual Review of Condensed Matter Physics* **5**, 57–82 (2014).
- <sup>9</sup> Shitade, A. *et al.* Quantum Spin Hall Effect in a Transition Metal Oxide  $\text{Na}_2\text{IrO}_3$ . *Physical Review Letters* **102**, 256403 (2009).
- <sup>10</sup> Guo, H. M. & Franz, M. Three-Dimensional Topological Insulators on the Pyrochlore Lattice. *Physical Review Letters* **103**, 206805 (2009).
- <sup>11</sup> Wan, X., Turner, A. M., Vishwanath, A. & Savrasov, S. Y. Topological semimetal and Fermi-arc surface states in the electronic structure of pyrochlore iridates. *Physical Review B* **83**, 205101 (2011).
- <sup>12</sup> Go, A., Witczak-Krempa, W., Jeon, G. S., Park, K. & Kim, Y. B. Correlation effects on 3D topological phases: from bulk to boundary. *Physical Review Letters* **109**, 066401 (2012).
- <sup>13</sup> Wan, X., Vishwanath, A. & Savrasov, S. Y. Computational Design of Axion Insulators Based on 5d Spinel Compounds. *Physical Review Letters* **108**, 146601 (2012).
- <sup>14</sup> Moon, E.-G., Xu, C., Kim, Y. B. & Balents, L. Non-fermi-liquid and topological states with strong spin-orbit coupling. *Physical Review Letters* **111**, 206401 (2013).
- <sup>15</sup> Maciejko, J., Chua, V. & Fiete, G. A. Topological Order in a Correlated Three-Dimensional Topological Insulator. *Physical Review Letters* **112**, 016404 (2014).
- <sup>16</sup> Okamoto, Y., Nohara, M., Aruga-Katori, H. & Takagi, H. Spin-Liquid State in the  $S=1/2$  Hyperkagome Antiferromagnet  $\text{Na}_4\text{Ir}_3\text{O}_8$ . *Physical Review Letters* **99**, 137207 (2007).
- <sup>17</sup> Chaloupka, J., Jackeli, G. & Khaliullin, G. Kitaev-Heisenberg Model on a Honeycomb Lattice: Possible Exotic Phases in Iridium Oxides  $A_2\text{IrO}_3$ . *Physical Review Letters* **105**, 027204 (2010).
- <sup>18</sup> Kim, B. J. *et al.* Novel  $J_{\text{eff}}=1/2$  Mott state induced by relativistic spin-orbit coupling in  $\text{Sr}_2\text{IrO}_4$ . *Physical Review Letters* **101**, 076402 (2008).
- <sup>19</sup> Kim, B. J. *et al.* Phase-Sensitive Observation of a Spin-Orbital Mott State in  $\text{Sr}_2\text{IrO}_4$ . *Science*

- 323**, 1329–1332 (2009).
- <sup>20</sup> Pocha, R., Johrendt, D. & Pöttgen, R. Electronic and Structural Instabilities in  $\text{GaV}_4\text{S}_8$  and  $\text{GaMo}_4\text{S}_8$ . *Chemistry of Materials* **12**, 2882 (2000).
- <sup>21</sup> Pocha, R., Johrendt, D., Ni, B. & Abd-Elmeguid, M. M. Crystal Structures, Electronic Properties, and Pressure-Induced Superconductivity of the Tetrahedral Cluster Compounds  $\text{GaNb}_4\text{S}_8$ ,  $\text{GaNb}_4\text{Se}_8$ , and  $\text{GaTa}_4\text{Se}_8$ . *Journal of the American Chemical Society* **127**, 8732 (2005).
- <sup>22</sup> Camjayi, A., Weht, R. & Rozenberg, M. Localised Wannier orbital basis for the Mott insulators  $\text{GaV}_4\text{S}_8$  and  $\text{GaTa}_4\text{Se}_8$ . *Europhysics Letters* **100**, 57004 (2012).
- <sup>23</sup> Ta Phuoc, V. *et al.* Optical Conductivity Measurements of  $\text{GaTa}_4\text{Se}_8$  under High Pressure: Evidence of a Bandwidth-Controlled Insulator-to-Metal Mott Transition. *Physical Review Letters* **110**, 037401 (2013).
- <sup>24</sup> Mazari, N. & Vanderbilt, D. Maximally-localized generalized Wannier functions for composite energy bands. *Physical Review B* **56**, 12847 (1997).
- <sup>25</sup> Souza, I., Mazari, N. & Vanderbilt, D. Maximally-localized Wannier functions for entangled energy bands. *Physical Review B* **65**, 035109 (2001).
- <sup>26</sup> Guiot, V., Janod, E., Corraze, B. & Cario, L. Control of the Electronic Properties and Resistive Switching in the New Series of Mott Insulators  $\text{GaTa}_4\text{Se}_{8-y}\text{Te}_y$  ( $0 \leq y \leq 6.5$ ). *Chemistry of Materials* **23**, 2611 (2011).
- <sup>27</sup> Francois, M. *et al.* Structural phase transition in  $\text{GaMo}_4\text{Se}_8$  and  $\text{AlMo}_4\text{S}_8$  by X-ray powder diffraction. *Zeitschrift für Kristallographie* **200**, 47 (1992).
- <sup>28</sup> Arita, R., Kuneš, J., Kozhevnikov, A., Eguiluz, A. & Imada, M. *Ab initio* studies on the interplay between spin-orbit interaction and Coulomb correlation in  $\text{Sr}_2\text{IrO}_4$  and  $\text{Ba}_2\text{IrO}_4$ . *Physical Review Letters* **108**, 086403 (2012).
- <sup>29</sup> Abd-Elmeguid, M. *et al.* Transition from Mott Insulator to Superconductor in  $\text{GaNb}_4\text{Se}_8$  and  $\text{GaTa}_4\text{Se}_8$  under High Pressure. *Physical Review Letters* **93**, 126403 (2004).
- <sup>30</sup> Zhang, H., Haule, K. & Vanderbilt, D. Effective  $J=1/2$  Insulating State in Ruddlesden-Popper Iridates: An LDA+DMFT Study. *Physical Review Letters* **111**, 246402 (2013).
- <sup>31</sup> Haldane, F. D. M. Model for a Quantum Hall Effect without Landau Levels: Condensed-Matter Realization of the “Parity Anomaly”. *Physical Review Letters* **61**, 2015 (1988).
- <sup>32</sup> Xiao, D., Zhu, W., Ran, Y., Nagaosa, N. & Okamoto, S. Interface engineering of quantum Hall effects in digital transition metal oxide heterostructures. *Nature Communications* **2**, 596

- (2011).
- <sup>33</sup> Dubost, V. *et al.* Resistive Switching at the Nanoscale in the Mott Insulator Compound GaTa<sub>4</sub>Se<sub>8</sub>. *Nano Letters* **13**, 3648 (2013).
- <sup>34</sup> Dubost, V. *et al.* Electric-Field-Assisted Nanostructuring of a Mott Insulator. *Advanced Functional Materials* **19**, 2800 (2009).
- <sup>35</sup> Micklitz, T. & Norman, M. R. Spin Hamiltonian of hyper-kagome Na<sub>4</sub>Ir<sub>3</sub>O<sub>8</sub>. *Physical Review B* **81**, 174417 (2010).
- <sup>36</sup> Jackeli, G. & Khaliullin, G. Mott Insulators in the Strong Spin-Orbit Coupling Limit: From Heisenberg to a Quantum Compass and Kitaev Models. *Physical Review Letters* **102**, 017205 (2009).
- <sup>37</sup> Nussinov, Z. & van den Brink, J. Compass and Kitaev models - Theory and Physical Motivations. Preprint at <http://arxiv.org/abs/1303.5922> (2013).
- <sup>38</sup> Jackeli, G. & Khaliullin, G. Magnetically Hidden Order of Kramers Doublets in  $d^1$  Systems: Sr<sub>2</sub>VO<sub>4</sub>. *Physical Review Letters* **103**, 067205 (2009).
- <sup>39</sup> Chen, G., Pereira, R. & Balents, L. Exotic phases induced by strong spin-orbit coupling in ordered double perovskites. *Physical Review B* **82**, 174440 (2010).
- <sup>40</sup> Pi, S.-T., Nanguneri, R. & Savrasov, S. Y. Calculation of Multipolar Exchange Interactions in Spin-Orbital Coupled Systems. *Physical Review Letters* **112**, 077203 (2014).
- <sup>41</sup> Jakob, S. *et al.* Structural and magnetic transitions in the Mott insulator GaNb<sub>4</sub>S<sub>8</sub>. *Journal of Material Chemistry* **17**, 3833 (2007).
- <sup>42</sup> Yamashita, S. *et al.* Thermodynamic properties of a spin-1/2 spin-liquid state in a  $\kappa$ -type organic salt. *Nature Physics* **4**, 459–462 (2008).
- <sup>43</sup> Kagawa, F., Miyagawa, K. & Kanoda, K. Magnetic Mott criticality in a  $\kappa$ -type organic salt probed by NMR. *Nature Physics* **5**, 880–884 (2009).
- <sup>44</sup> Yamashita, M. *et al.* Highly Mobile Gapless Excitations in a Two-Dimensional Candidate Quantum Spin Liquid. *Science* **328**, 1246–1248 (2010).
- <sup>45</sup> Perdew, J. P. *et al.* Restoring the Density-Gradient Expansion for Exchange in Solids and Surfaces. *Physical Review Letters* **100**, 136406 (2008).
- <sup>46</sup> Kresse, G. & Hafner, J. *Ab initio* molecular dynamics for liquid metals. *Physical Review B* **47**, 558 (1993).
- <sup>47</sup> Kresse, G. & Furthmüller, J. Efficient iterative schemes for *ab initio* total-energy calculations

- using a plane-wave basis set. *Physical Review B* **54**, 11169 (1996).
- <sup>48</sup> Ozaki, T. Variationally optimized atomic orbitals for large-scale electronic structures. *Physical Review B* **67**, 155108 (2003).
- <sup>49</sup> Dudarev, S., Botton, G., Savrasov, S., Humphreys, C. & Sutton, A. Electron-energy-loss spectra and the structural stability of nickel oxide:An LSDA+ $U$  study. *Physical Review B* **57**, 1505 (1998).
- <sup>50</sup> Han, M. J., Ozaki, T. & Yu, J. O(N) LDA+ $U$  electronic structure calculation method based on the nonorthogonal pseudoatomic orbital basis. *Physical Review B* **73**, 045110 (2006).

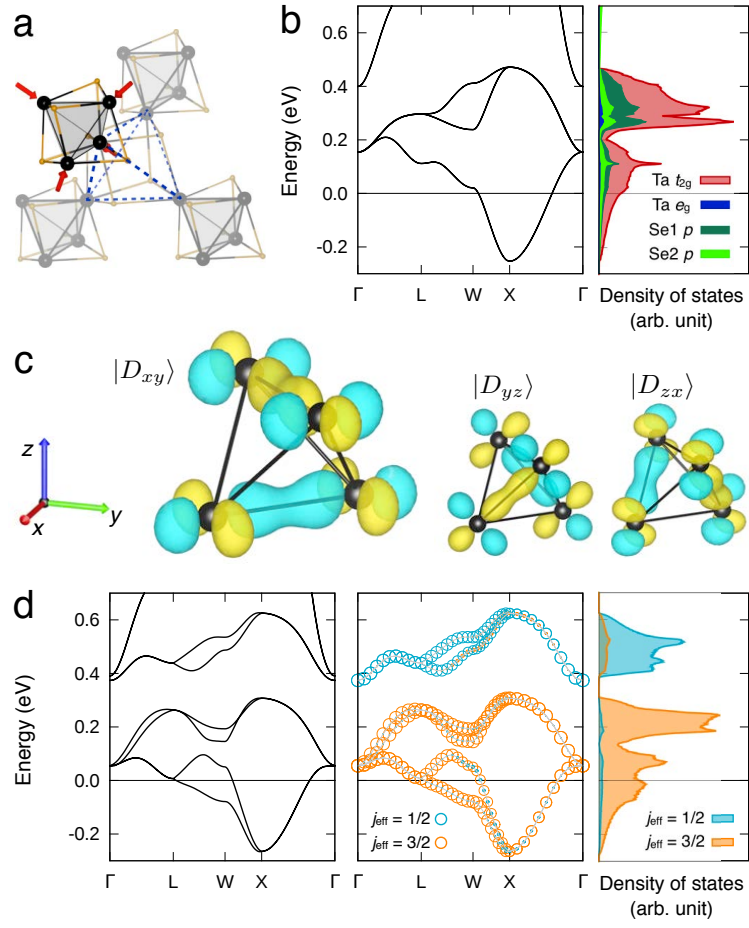


FIG. 1.

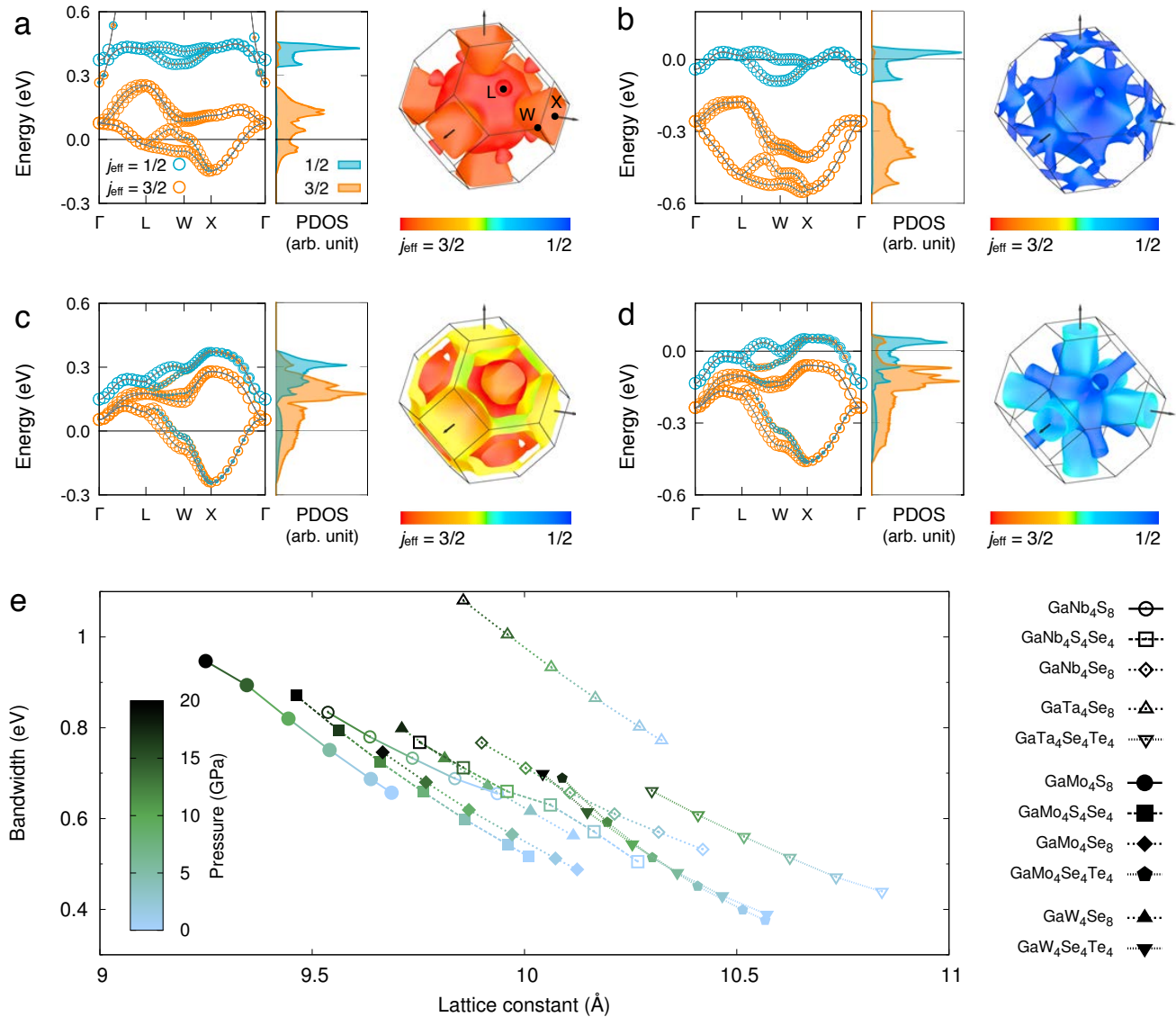


FIG. 2.

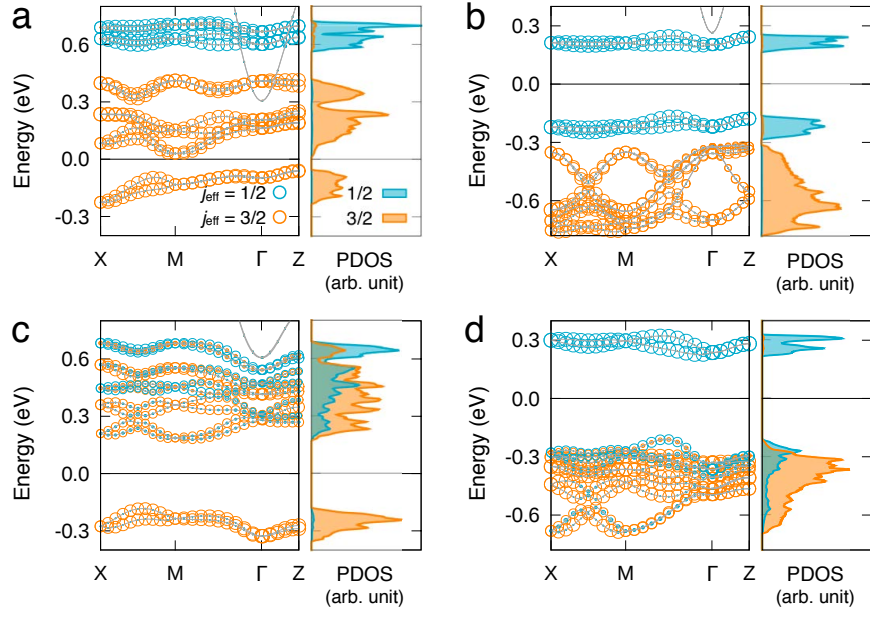


FIG. 3.

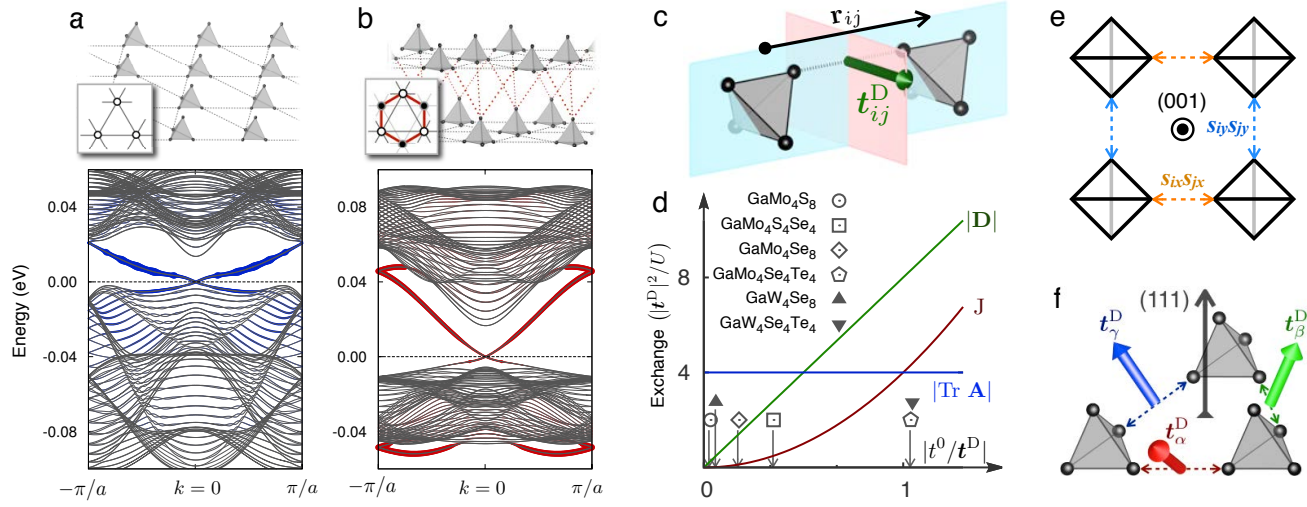


FIG. 4.



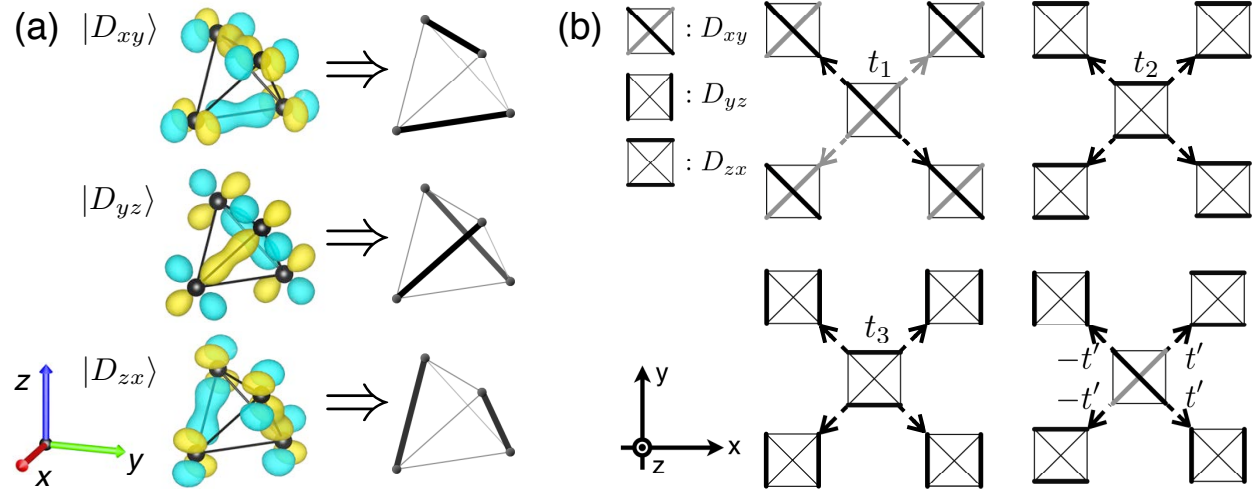
**Figure 1 | Molecular form of spin-orbital entangled  $j_{\text{eff}}$  states in GaTa<sub>4</sub>Se<sub>8</sub>.** **a** The connectivity between the neighboring  $M_4$  clusters and the local distortion of each cluster. **b** Band structure and projected density of states of GaTa<sub>4</sub>Se<sub>8</sub> without SOC. **c** Three Wannier orbitals constructed from the triplet molecular orbital bands near the Fermi level. **d** Band structure and density of states with SOC, projected onto the  $j_{\text{eff}} = 1/2$  and  $3/2$  subspaces. The size of the circle in the band structure shows the weight of each subspace in each Bloch state.

**Figure 2 |  $j_{\text{eff}}$ -ness in the GaM<sub>4</sub>X<sub>8</sub> series.** The molecular  $j_{\text{eff}}$ -projected band structures, density of states, and the Fermi surfaces of **a** GaTa<sub>4</sub>Se<sub>4</sub>Te<sub>4</sub>, **b** GaW<sub>4</sub>Se<sub>4</sub>Te<sub>4</sub>, **c** GaNb<sub>4</sub>Se<sub>8</sub>, and **d** GaMo<sub>4</sub>Se<sub>8</sub> are presented. **e** The relation between the external hydrostatic pressure, lattice constant, and bandwidth of the molecular  $t_2$  bands in the absence of SOC.

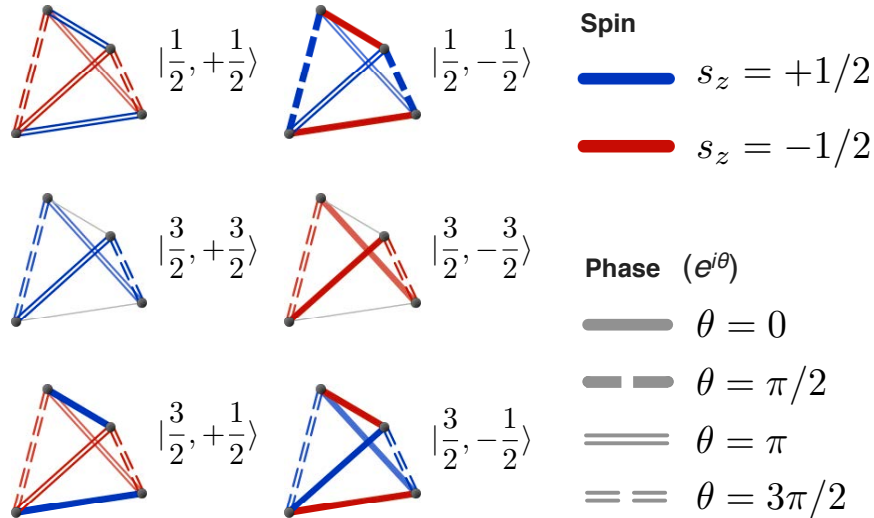
**Figure 3 | DFT+SOC+ $U$  calculations.** The  $j_{\text{eff}}$ -projected band structure and density of states of **a** GaTa<sub>4</sub>Se<sub>4</sub>Te<sub>4</sub>, **b** GaW<sub>4</sub>Se<sub>4</sub>Te<sub>4</sub>, **c** GaNb<sub>4</sub>Se<sub>8</sub>, and **d** GaMo<sub>4</sub>Se<sub>8</sub> with the presence of electron correlations and antiferromagnetic order.

**Figure 4 | Topological insulating phases and anisotropic spin model.** The one-dimensional band structure of **a** half-filled  $j_{\text{eff}} = 3/2$  monolayer and **b** half-filled  $j_{\text{eff}} = 1/2$  bilayer  $M_4$  ribbons (20 unit cell width). The insets show schematic top view of each system, where the thin grey and the thick red lines represent the intra- and the inter-planar bonding, respectively. The thickness of the colored fat lines in the band structure represent the weights on the edge. **c** Two mirror planes (blue and red) existing in between the neighboring  $M_4$  clusters determine the direction of  $\mathbf{t}_{ij}^D$  illustrated as green arrow. **d** Magnitudes of Heisenberg (dark red), Dzyaloshinskii-Moriya (green), and pseudodipolar (blue) exchange interactions as a function of  $|t_0/\mathbf{t}^D|$ . The magnitude of  $|t_0/\mathbf{t}^D|$  for each of the  $M = \text{Mo/W}$  compounds is marked on the horizontal axis. **e** The 90°- and **f** the 60°- compass interactions are realized on (001) and (111)  $M_4$  monolayers, respectively.

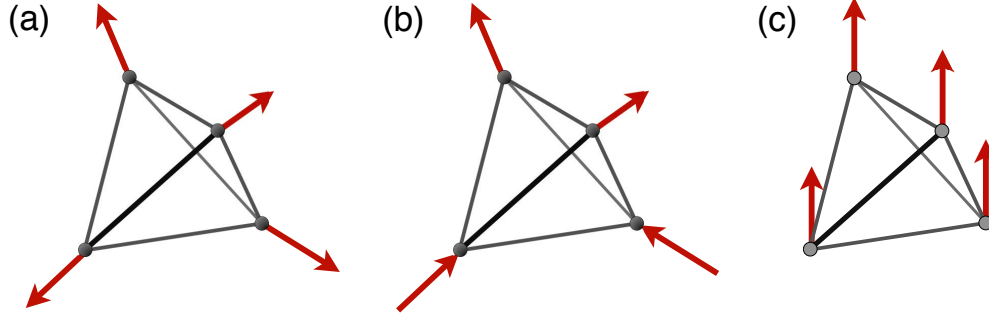
## Supplementary Figures



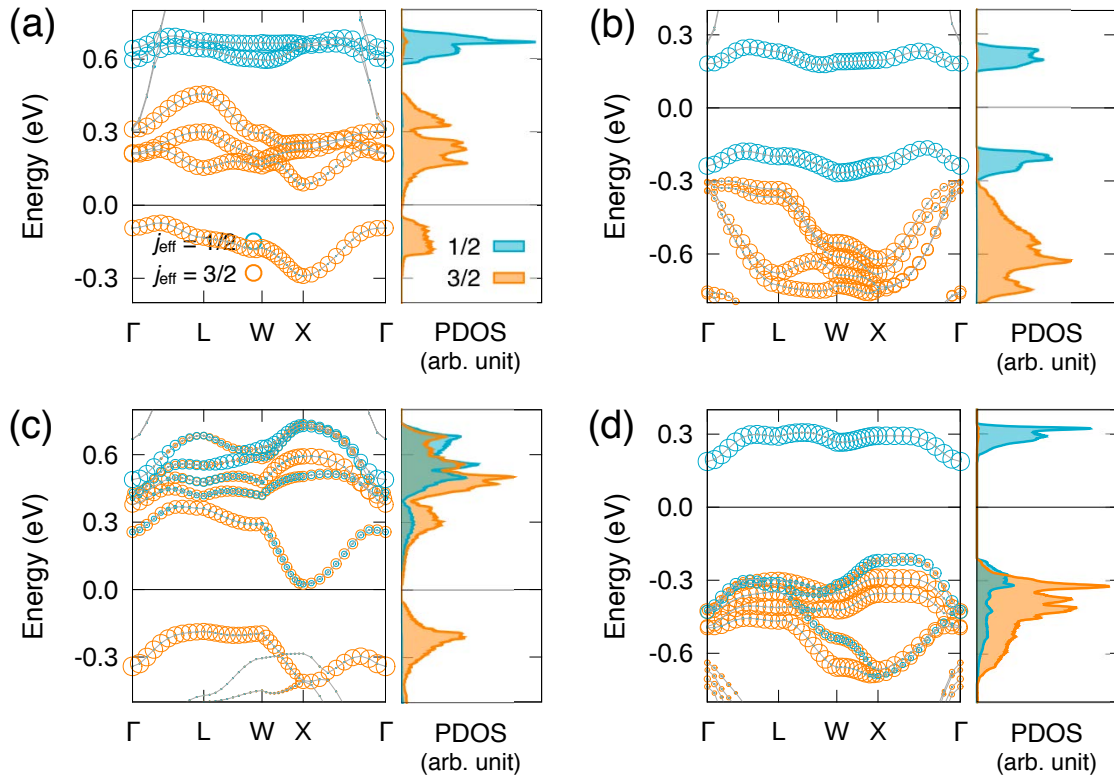
**Supplementary Figure 1: Molecular  $t_2$  orbitals and hopping channels.** (a) The molecular  $t_2$  orbitals and their schematic representations. (b) Four nearest-neighbor hopping channels  $-t_1$ ,  $t_2$ ,  $t_3$ , and  $t'$  between the molecular  $t_2$  orbitals on the  $xy$ -plane.



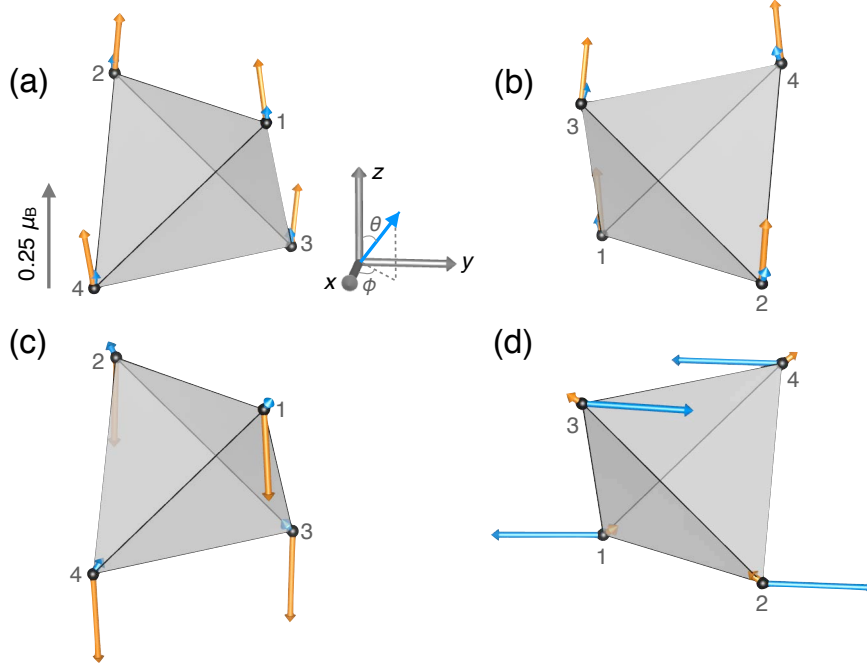
**Supplementary Figure 2: Molecular  $j_{\text{eff}}$  orbitals.** Schematic viewgraph of the molecular  $j_{\text{eff}}$  orbitals. Color and type of the thick lines represent the spin component and the phase factor assigned to the constituent molecular  $t_2$  orbitals.



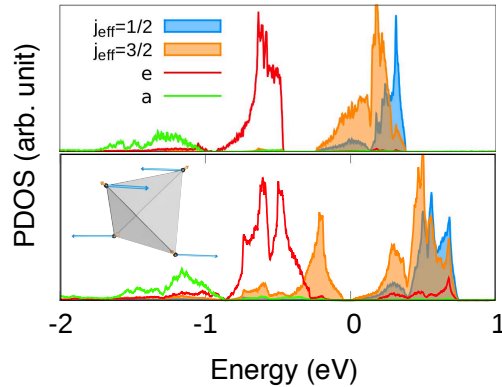
**Supplementary Figure 3: Initial non-collinear magnetic configurations.** Three initial magnetic configurations within the  $M_4$  cluster used in the DFT+SOC+ $U$  calculations: (a) the all-in-all-out, (b) the 2-in-2-out, and (c) the collinear order.



**Supplementary Figure 4:  $j_{\text{eff}}$ -projected electronic structures with ferromagnetic order.** The  $j_{\text{eff}}$ -projected band structures and PDOS of (a)  $\text{GaTa}_4\text{Se}_4\text{Te}_4$ , (b)  $\text{GaW}_4\text{Se}_4\text{Te}_4$ , (c)  $\text{GaNb}_4\text{Se}_8$ , and (d)  $\text{GaMo}_4\text{Se}_8$  with the presence of electron correlations and ferromagnetic order.



**Supplementary Figure 5: Magnetic ordering in a  $M_4$  cluster.** The spin (blue) and orbital (orange) angular momenta at the  $M_4$  corners of (a)  $\text{GaW}_4\text{Se}_4\text{Te}_4$ , (b)  $\text{GaMo}_4\text{Se}_8$ , (c)  $\text{GaTa}_4\text{Se}_4\text{Te}_4$ , and (d)  $\text{GaNb}_4\text{Se}_8$  from the FM results (Supplementary Figure 4).  $M_4$  site indices for each compound ( $i = 1, \dots, 4$ ) are shown.



**Supplementary Figure 6: PDOS of  $\text{GaNb}_4\text{Se}_8$  projected onto the molecular states.** Top and bottom panel show PDOS from the paramagnetic result at  $U_{\text{eff}} = 0.0$  eV and the non-collinear order at  $U_{\text{eff}} = 2.5$  eV, respectively. The inset in the lower panel shows SAM (blue) and OAM (orange) within the  $M_4$  cluster.

## Supplementary Tables

	$P$ (GPa)	$t_1$	$t_2$	$t_3$	$t'$ (meV)
GaNb <sub>4</sub> S <sub>8</sub>	0	-60.5	30.9	4.3	16.7
	21	-86.3	44.7	11.0	18.7
GaNb <sub>4</sub> S <sub>4</sub> Se <sub>4</sub>	0	-33.4	22.4	1.6	15.7
	20	-50.6	32.9	4.3	17.4
GaNb <sub>4</sub> Se <sub>8</sub>	0	-41.5	22.8	0.6	15.1
	15	-89.3	48.5	15.4	23.4
GaMo <sub>4</sub> S <sub>8</sub>	0	-48.0	24.9	7.4	19.9
	20	-63.7	36.9	14.4	23.2
GaMo <sub>4</sub> S <sub>4</sub> Se <sub>4</sub>	0	-22.9	20.4	3.1	18.1
	22	-34.0	30.3	6.9	19.6
GaMo <sub>4</sub> Se <sub>8</sub>	0	-31.0	19.7	2.8	16.7
	19	-45.9	28.8	8.2	18.9
GaMo <sub>4</sub> Se <sub>4</sub> Te <sub>4</sub>	0	-4.4	16.9	3.7	10.0
	17	-3.6	26.6	5.0	8.2
GaTa <sub>4</sub> Se <sub>8</sub>	0	-55.7	27.6	7.1	14.5
	20	-75.5	37.1	8.4	15.1
GaTa <sub>4</sub> Se <sub>4</sub> Te <sub>4</sub>	0	-22.9	17.1	12.0	9.2
	15	-33.8	24.5	15.7	8.2
GaW <sub>4</sub> Se <sub>8</sub>	0	-42.3	22.6	7.3	16.7
	21	-64.6	33.0	3.0	18.9
GaW <sub>4</sub> Se <sub>4</sub> Te <sub>4</sub>	0	-14.6	18.3	11.0	9.7
	20	-20.6	23.6	16.6	8.9

**Supplementary Table 1: Molecular  $t_2$  hopping terms.** NN hopping terms between the molecular  $t_2$  orbitals of the lacunar spinel compounds, with/without the external pressure.

$U_{\text{eff}}$ (eV)	$i$	FM						AFM						$\Delta E$ (meV)
		$ S $	$\theta_S$	$\phi_S$	$ L $	$\theta_L$	$\phi_L$	$ S $	$\theta_S$	$\phi_S$	$ L $	$\theta_L$	$\phi_L$	
1.0	1	0.041	2.5	225.0	0.125	8.3	225.0	0.032	30.4	44.9	0.103	29.7	44.9	2.9
	2	0.041	6.2	45.0	0.127	11.5	45.0	0.042	35.2	44.9	0.139	35.3	44.9	
	3	0.041	4.8	109.6	0.126	10.2	122.6	0.040	37.8	55.6	0.129	38.1	55.6	
	4	0.041	4.8	-19.6	0.126	10.2	-32.6	0.040	37.8	34.3	0.129	38.1	34.3	
1.5	1	0.044	5.5	45.0	0.139	4.9	225.0	0.038	33.6	46.4	0.117	29.7	46.9	-0.3
	2	0.045	6.7	45.0	0.149	14.9	45.0	0.044	35.4	46.2	0.158	35.4	46.2	
	3	0.044	6.2	50.6	0.144	12.1	100.8	0.043	36.5	51.9	0.148	38.4	56.9	
	4	0.044	6.2	39.4	0.144	12.1	-10.8	0.043	36.4	40.3	0.147	38.3	35.0	
2.0	1	0.047	3.7	45.0	0.160	11.4	225.0	0.046	37.8	47.0	0.127	29.9	48.5	-0.01
	2	0.047	6.7	225.0	0.158	9.0	45.0	0.043	35.9	47.2	0.174	35.6	47.2	
	3	0.047	5.4	-59.7	0.159	10.3	144.1	0.044	34.6	45.0	0.163	38.8	57.9	
	4	0.047	5.4	149.7	0.159	10.3	-54.1	0.044	34.6	49.7	0.162	38.7	35.6	

**Supplementary Table 2: Magnetism in GaW<sub>4</sub>Se<sub>4</sub>Te<sub>4</sub>.** Sizes (in  $\mu_B$ ) and directions (in degree) of SAM and OAM on the four corners of the  $M_4$  cluster for the FM and AFM configurations, the energy difference  $\Delta E \equiv E_{\text{AFM}} - E_{\text{FM}}$ , and their  $U_{\text{eff}}$  dependence in GaW<sub>4</sub>Se<sub>4</sub>Te<sub>4</sub>. See Supplementary Figure 5 for the definitions of angle  $\theta$ ,  $\phi$ , and site index  $i$ .

$U_{\text{eff}}$ (eV)	$i$	FM						AFM						$\Delta E$ (meV)
		$ S $	$\theta_S$	$\phi_S$	$ L $	$\theta_L$	$\phi_L$	$ S $	$\theta_S$	$\phi_S$	$ L $	$\theta_L$	$\phi_L$	
1.5	1	0.048	24.4	225.0	0.129	7.0	225.0	0.016	33.3	225.3	0.114	31.0	44.9	-0.2
	2	0.048	24.6	45.0	0.129	7.2	45.0	0.056	34.8	44.9	0.137	35.4	44.9	
	3	0.048	24.5	134.6	0.129	7.1	133.9	0.054	50.1	80.5	0.129	37.6	51.4	
	4	0.048	24.5	-44.6	0.129	7.1	-43.9	0.054	50.1	9.5	0.129	37.6	38.4	
2.0	1	0.049	24.7	224.8	0.146	6.3	224.4	0.017	38.5	226.9	0.127	31.1	44.3	-0.1
	2	0.050	25.4	45.2	0.147	7.9	45.5	0.058	35.1	44.4	0.154	35.5	44.5	
	3	0.050	25.1	132.3	0.147	7.2	126.8	0.057	50.6	81.0	0.146	37.6	51.5	
	4	0.050	25.0	-42.3	0.147	7.1	-36.7	0.057	50.4	8.8	0.146	37.7	37.6	
2.5	1	0.051	24.0	225.0	0.164	7.1	225.0	0.017	42.3	226.8	0.140	31.3	44.3	-0.1
	2	0.051	23.9	45.0	0.164	7.0	45.0	0.059	35.4	44.5	0.170	35.6	44.5	
	3	0.051	24.0	135.2	0.164	7.1	135.5	0.059	50.3	81.5	0.161	37.8	51.7	
	4	0.051	24.0	-45.2	0.164	7.1	-45.5	0.060	50.2	8.3	0.161	37.9	37.4	

**Supplementary Table 3: Magnetism in GaMo<sub>4</sub>Se<sub>8</sub>.**

$U_{\text{eff}}$ (eV)	$i$	FM						AFM						$\Delta E$ (meV)
		$ S $	$\theta_S$	$\phi_S$	$ L $	$\theta_L$	$\phi_L$	$ S $	$\theta_S$	$\phi_S$	$ L $	$\theta_L$	$\phi_L$	
1.0		Paramagnetic												—
	1	0.033	27.9	45.0	0.165	175.9	45.0	0.038	35.6	225.0	0.051	149.6	45.0	
1.5	2	0.034	29.2	226.0	0.165	176.8	225.0	0.028	37.8	225.0	0.036	158.8	45.0	-1.6
	3	0.034	28.8	-46.7	0.165	176.3	-37.9	0.036	38.9	210.2	0.055	140.0	38.4	
	4	0.033	28.3	135.7	0.165	176.3	127.9	0.036	38.9	239.8	0.055	140.0	51.6	
	1	0.049	43.1	45.0	0.229	176.9	45.0	0.140	21.1	225.0	0.226	156.7	45.0	
2.0	2	0.049	42.8	225.0	0.229	176.9	225.0	0.121	28.3	225.0	0.222	167.6	45.0	6.5
	3	0.049	43.0	-44.8	0.229	176.9	-45.0	0.112	2.4	0.3	0.221	162.8	24.0	
	4	0.049	43.0	134.8	0.229	176.9	135.0	0.112	2.4	89.8	0.221	162.8	66.0	

**Supplementary Table 4: Magnetism in GaTa<sub>4</sub>Se<sub>4</sub>Te<sub>4</sub>.**

$U_{\text{eff}}$ (eV)	$i$	FM						AFM						$\Delta E$ (meV)
		$ S $	$\theta_S$	$\phi_S$	$ L $	$\theta_L$	$\phi_L$	$ S $	$\theta_S$	$\phi_S$	$ L $	$\theta_L$	$\phi_L$	
1.5		Paramagnetic												—
	1	0.190	125.3	225.0	0.119	16.2	225.0	0.196	58.9	225.0	0.029	161.8	45.0	
2.0	2	0.112	140.5	225.0	0.128	18.9	45.0	0.137	82.1	45.0	0.104	141.9	225.0	-17.4
	3	0.112	116.8	239.7	0.124	17.9	125.4	0.094	83.1	7.0	0.078	130.6	235.9	
	4	0.112	116.8	210.3	0.124	17.9	-35.4	0.094	83.1	83.0	0.078	130.6	214.1	
	1	0.269	90.5	-87.0	0.047	56.0	72.2	0.294	110.2	-87.9	0.061	56.1	70.3	
2.5	2	0.269	91.6	93.1	0.048	55.7	252.0	0.328	45.0	90.0	0.011	135.0	270.0	-10.6
	3	0.269	91.8	86.9	0.048	55.6	-72.1	0.175	45.0	90.0	0.003	135.0	-90.0	
	4	0.268	90.5	267.0	0.047	56.0	107.9	0.294	159.7	264.2	0.061	38.6	116.7	

**Supplementary Table 5: Magnetism in GaNb<sub>4</sub>Se<sub>8</sub>.**

## Supplementary Notes

**Supplementary Note 1: Molecular  $t_2$  Hopping Terms.** In this section, we construct the tight-binding Hamiltonian based on the molecular  $t_2$  states in the absence of spin-orbit coupling (SOC). Regarding only the nearest-neighboring (NN) sites  $i$  and  $j$ , the tight-binding Hamiltonian can be written as

$$\mathcal{H}_{\text{hopping};ij}^{t_2} = \begin{pmatrix} S_1 & S_5 - A_2 & S_4 + A_1 \\ S_5 + A_2 & S_2 & S_6 - A_3 \\ S_4 - A_1 & S_6 + A_3 & S_3 \end{pmatrix} \quad (5)$$

in terms of the basis set  $(D_{xy}, D_{yz}, D_{zx})$ . Here,  $S$  and  $A$  denote symmetric and antisymmetric hopping terms with respect to the site inversion  $i \leftrightarrow j$  such that  $\mathcal{H}_{\text{hopping};ji}^{t_2} = \mathcal{H}_{\text{hopping};ij}^{t_2}(-A)$ , or equivalently  $(\mathcal{H}_{\text{hopping};ij}^{t_2})^T = \mathcal{H}_{\text{hopping};ji}^{t_2}$ .

Wannier function analysis shows that only 4 NN hopping channels – say,  $t_1$ ,  $t_2$ ,  $t_3$ , and  $t'$  – are allowed in the  $AM_4X_8$  compounds. The edge-sharing geometry of the distorted  $MX_8$  octahedra enables the correspondence of our  $t_1$ ,  $t_2$ , and  $t_3$  hopping terms to those in the layered iridates  $A_2\text{IrO}_3$  ( $A = \text{Li}, \text{Na}$ )<sup>1,2</sup> as shown schematically in Supplementary Figure 1;  $t_1$ ,  $t_2$ , and  $t_3$  correspond to  $t_{dd1}$  ( $\sigma$ -type),  $t_{pd}$  ( $\pi$ -type), and  $t_{dd2}$  ( $\delta$ -type) hopping integrals in Supplementary Reference 1, respectively. The antisymmetric term  $t'$  is allowed due to the lack of inversion symmetry by the formation of the  $M_4$  clusters. Along the direction to the 12 NNs in the face-centered cubic lattice, *i.e.*  $\mathbf{r}_{ij} = n_1\mathbf{a}_1 + n_2\mathbf{a}_2 + n_3\mathbf{a}_3$ , the NN hopping terms are as follows:

$$(n_1, n_2, n_3) = (\pm 1, \mathbf{0}, \mathbf{0}) \quad S_1 = t_1, \quad S_2 = S_3 = t_2, \quad S_6 = -t_3, \quad A_1 = -A_2 = \mp t'$$

$$(n_1, n_2, n_3) = (\mathbf{0}, \pm 1, \mathbf{0}) \quad S_1 = S_3 = t_2, \quad S_2 = t_1, \quad S_4 = -t_3, \quad A_2 = -A_3 = \mp t'$$

$$(n_1, n_2, n_3) = (\mathbf{0}, \mathbf{0}, \pm 1) \quad S_1 = S_2 = t_2, \quad S_3 = t_1, \quad S_5 = -t_3, \quad A_1 = -A_3 = \pm t'$$

$$(n_1, n_2, n_3) = (\pm 1, \mp 1, \mathbf{0}) \quad S_1 = S_2 = t_2, \quad S_3 = t_1, \quad S_5 = t_3, \quad A_1 = A_3 = \pm t'$$

$$(n_1, n_2, n_3) = (\mathbf{0}, \pm 1, \mp 1) \quad S_1 = t_1, \quad S_2 = S_3 = t_2, \quad S_6 = t_3, \quad A_1 = A_2 = \pm t'$$

$$(n_1, n_2, n_3) = (\pm 1, \mathbf{0}, \mp 1) \quad S_1 = S_3 = t_2, \quad S_2 = t_1, \quad S_4 = t_3, \quad A_2 = A_3 = \mp t'$$

Here we adopt the convention that  $t_3, t' > 0$ . The other terms not shown above are all zero. The amount of each hopping term, with and without external pressure, is shown in Supplementary Table 1. The values of the NN hopping terms for  $\text{GaTa}_4\text{Se}_8$ , in the absence



of external pressure, are consistent with the previous work<sup>3</sup>.

**Supplementary Note 2: Molecular  $j_{\text{eff}}$  Hopping Terms in the Presence of SOC.** As mentioned in the main text, the molecular  $t_2$  states behave in the same way as the atomic  $t_{2g}$  states do under SOC<sup>4</sup>. The SOC Hamiltonian is written as

$$\mathcal{H}_{\text{SO}} \equiv \lambda_{\text{SO}} \mathbf{L} \cdot \mathbf{S}. \quad (6)$$

where  $\lambda_{\text{SO}}$  is the SOC strength of the transition metal atoms, and  $\mathbf{L}$  and  $\mathbf{S}$  are the orbital and the spin angular momentum operators, respectively.

The eigenstates of the SOC Hamiltonian in Eq. (6) are written as

$$\begin{aligned} |j_{\text{eff}} = \frac{1}{2}; \pm \frac{1}{2}\rangle &= \mp \frac{1}{\sqrt{3}} (|D_{xy}, \uparrow\downarrow\rangle \pm |D_{yz}, \downarrow\uparrow\rangle + i|D_{zx}, \downarrow\uparrow\rangle) \\ |j_{\text{eff}} = \frac{3}{2}; \pm \frac{1}{2}\rangle &= \sqrt{\frac{2}{3}} \left[ |D_{xy}, \uparrow\downarrow\rangle \mp \frac{|D_{yz}, \downarrow\uparrow\rangle \pm i|D_{zx}, \downarrow\uparrow\rangle}{2} \right] \\ |j_{\text{eff}} = \frac{3}{2}; \pm \frac{3}{2}\rangle &= \mp \frac{1}{\sqrt{2}} (|D_{yz}, \uparrow\downarrow\rangle \pm i|D_{zx}, \uparrow\downarrow\rangle), \end{aligned} \quad (7)$$

which are schematically shown in Supplementary Figure 2. By adding SOC to the molecular  $t_2$  Hamiltonian in Eq. (5) and transforming the molecular  $t_2$  into the  $j_{\text{eff}}$  basis sets, Hamiltonian now has the following form:

$$\mathcal{H}^{j_{\text{eff}}} = \left( \begin{array}{cc|cc} +\lambda_{\text{SO}} \mathbf{I}^{1/2} & & \mathbf{T}_{ij}^{1/2} & \Theta_{ij} \\ & -\frac{1}{2} \lambda_{\text{SO}} \mathbf{I}^{3/2} & \Theta_{ij} (-A)^\dagger & \mathbf{T}_{ij}^{3/2} \\ \hline \mathbf{T}_{ji}^{1/2} & \Theta_{ji} & +\lambda_{\text{SO}} \mathbf{I}^{1/2} & \\ \Theta_{ji} (-A)^\dagger & \mathbf{T}_{ji}^{3/2} & & -\frac{1}{2} \lambda_{\text{SO}} \mathbf{I}^{3/2} \end{array} \right) \quad (8)$$

where  $\mathbf{I}^{1/2, 3/2}$  are the identity matrices for the  $j_{\text{eff}} = 1/2$  and  $3/2$  subspaces, respectively. The hopping terms within the  $j_{\text{eff}} = 1/2$  and  $3/2$  subspaces,  $\mathbf{T}_{ij}^{1/2, 3/2}$ , are written in terms of the molecular  $t_2$  hopping terms in Eq. (5) such that

$$\begin{aligned} \mathbf{T}_{ij}^{1/2} &= t^0 \mathbf{I} + i \mathbf{t}_{ij}^{\text{D}} \cdot \mathbf{S}^{1/2} \\ \mathbf{T}_{ij}^{3/2} &= t^0 \mathbf{I} + i \mathbf{t}_{ij}^{\text{D}} \cdot \mathbf{S}^{3/2} + \mathbf{t}_{ij}^{\text{Q}} \cdot \mathbf{\Gamma} \end{aligned}$$

$$\begin{aligned}
\text{where } t^0 &= \frac{1}{3} (S_1 + S_2 + S_3), \\
\mathbf{t}^D &= -\frac{2}{3} (A_1, A_2, A_3), \\
\mathbf{t}^Q &= -\frac{1}{\sqrt{3}} \left( S_4, S_5, S_6, \frac{S_2 - S_3}{2}, \frac{2S_1 - S_2 - S_3}{2\sqrt{3}} \right),
\end{aligned}$$

and  $\mathbf{S}^{1/2}$  and  $\mathbf{S}^{3/2}$  are the pseudospin operators of the  $j_{\text{eff}} = 1/2$  and  $3/2$  states, respectively.  $\mathbf{t}^D$  couples to  $\mathbf{S}^{1/2,3/2}$  and can be interpreted as the effective dipolar fields on the hopping electrons, of which directions are shown in Fig. 4 **c** in the main text. For the  $j_{\text{eff}} = 3/2$  states, additional quadrupolar fields manifested as the Dirac Gamma matrices  $\Gamma \equiv (\Gamma_1, \Gamma_2, \Gamma_3, \Gamma_4, \Gamma_5)$  couple to the hopping electron, where the Dirac matrices are defined as<sup>5</sup>  $\Gamma_1 = \sigma^z \otimes \sigma^y$ ,  $\Gamma_2 = \sigma^z \otimes \sigma^x$ ,  $\Gamma_3 = \sigma^y \otimes \mathbf{I}^{1/2}$ ,  $\Gamma_4 = \sigma^x \otimes \mathbf{I}^{1/2}$ ,  $\Gamma_5 = \sigma^z \otimes \sigma^z$ . Note that the Dirac Gamma matrices can be represented in terms of  $\mathbf{S}^{3/2}$  such that

$$\Gamma = \left( \sqrt{3}\{S_y^{3/2}, S_z^{3/2}\}, \sqrt{3}\{S_z^{3/2}, S_x^{3/2}\}, \sqrt{3}\{S_x^{3/2}, S_y^{3/2}\}, \frac{1}{\sqrt{3}} [(S_x^{3/2})^2 - (S_y^{3/2})^2], (S_z^{3/2})^2 \right).$$

The inter-orbital hopping term  $\Theta_{ij}$  is given as

$$\Theta_{ij} \equiv \begin{pmatrix} \frac{(S_4+A_1)-i(S_5+A_2)}{\sqrt{6}} & \frac{(2S_1-S_2-S_3)+2iA_3}{3\sqrt{2}} & \frac{(3S_4-A_1)+i(3S_5-A_2)}{3\sqrt{2}} & \frac{(S_2-S_3)+2iS_6}{\sqrt{6}} \\ \frac{(-S_2+S_3)+2iS_6}{\sqrt{6}} & \frac{-(3S_4-A_1)+i(3S_5-A_2)}{3\sqrt{2}} & \frac{(2S_1-S_2-S_3)-2iA_3}{3\sqrt{2}} & \frac{(S_4+A_1)+i(S_5+A_2)}{\sqrt{6}} \end{pmatrix}.$$

Note that, from the hermiticity,  $\Theta_{ij}(-A) = \Theta_{ji}$ .

**Supplementary Note 3: Block-diagonalization of  $j_{\text{eff}}$ -based Effective Hamiltonian.** Rearranging the Hamiltonian in Eq. (8) in terms of the  $j_{\text{eff}} = 1/2$  and  $3/2$  subspaces yields

$$\mathcal{H}^{j_{\text{eff}}} = \left( \begin{array}{cc|cc} +\lambda_{\text{SO}}\mathbf{I}^{1/2} & \mathbf{T}_{ij}^{1/2} & & \Theta_{ij} \\ \mathbf{T}_{ji}^{1/2} & +\lambda_{\text{SO}}\mathbf{I}^{1/2} & \Theta_{ji} & \\ \hline & \Theta_{ij}(-A)^\dagger & -\frac{1}{2}\lambda_{\text{SO}}\mathbf{I}^{3/2} & \mathbf{T}_{ij}^{3/2} \\ \Theta_{ji}(-A)^\dagger & & \mathbf{T}_{ji}^{3/2} & -\frac{1}{2}\lambda_{\text{SO}}\mathbf{I}^{3/2} \end{array} \right). \quad (9)$$

As the energy splitting between the  $j_{\text{eff}} = 1/2$  and  $3/2$  states,  $\frac{3}{2}\lambda_{\text{SO}}$ , is large compared to the inter-orbital hopping terms  $\Theta$ , we can block-diagonalize  $\mathcal{H}^{j_{\text{eff}}}$  into the  $j_{\text{eff}} = 1/2$  and  $3/2$

subspaces. The correction to the  $j_{\text{eff}} = 1/2$  on-site terms are as follows:

$$\begin{aligned}
\Delta\mathcal{H}_{11}^{j_{\text{eff}}} &= \frac{2}{3\lambda_{\text{SO}}} \sum_{n=5}^{12} \mathcal{H}_{1n}^{j_{\text{eff}}} \mathcal{H}_{n1}^{j_{\text{eff}}} \\
&= \frac{4}{27\lambda_{\text{SO}}} [(S_1^2 + S_2^2 + S_3^2 - S_1S_2 - S_2S_3 - S_3S_1) + 3(S_4^2 + S_5^2 + S_6^2) + (A_1^2 + A_2^2 + A_3^2)] \\
\Delta\mathcal{H}_{12}^{j_{\text{eff}}} &= \frac{2}{3\lambda_{\text{SO}}} \sum_{n=5}^{12} \mathcal{H}_{1n}^{j_{\text{eff}}} \mathcal{H}_{n2}^{j_{\text{eff}}} \\
&= \frac{2}{3\lambda_{\text{SO}}} \left\{ \frac{1}{6} [(S_5 - A_2) + i(S_4 + A_1)] [(S_2 - A_3) - 2iS_6] \right. \\
&\quad + \frac{1}{18} [(2S_1 - S_2 - S_3) + 2iA_3] [(3S_5 + A_2) - i(3S_4 - A_1)] \\
&\quad + \frac{1}{18} [(2S_1 - S_2 - S_3) + 2iA_3] [-(3S_5 + A_2) + i(3S_4 - A_1)] \\
&\quad \left. + \frac{1}{6} [(S_5 - A_2) + i(S_4 + A_1)] [(-S_2 + A_3) + 2iS_6] \right\} = 0
\end{aligned}$$

Straightforward calculations for other diagonal terms yield  $\Delta\mathcal{H}_{11}^{j_{\text{eff}}} = \Delta\mathcal{H}_{22}^{j_{\text{eff}}} = \Delta\mathcal{H}_{33}^{j_{\text{eff}}} = \Delta\mathcal{H}_{44}^{j_{\text{eff}}}$ , and the off-diagonal terms vanish ( $\Delta\mathcal{H}_{12}^{j_{\text{eff}}} = \Delta\mathcal{H}_{21}^{j_{\text{eff}}} = \Delta\mathcal{H}_{34}^{j_{\text{eff}}} = \Delta\mathcal{H}_{43}^{j_{\text{eff}}} = 0$ ). For the  $4d$  transition metal compounds, especially for  $\text{GaMo}_4\text{S}_8$ , the on-site energy shift from this inter-subspace mixing is less than 20 meV, which is an order-of-magnitude smaller than the the SOC splitting. In the  $5d$  transition metal compounds, the correction becomes negligible.

Similarly, the corrections to the hopping term,  $\mathbf{T}_{ij}^{1/2}$ , are as follows:

$$\begin{aligned}
\Delta\mathcal{H}_{13}^{j_{\text{eff}}} &= \frac{2}{3\lambda_{\text{SO}}} \sum_{n=5}^{12} \mathcal{H}_{1n}^{j_{\text{eff}}} \mathcal{H}_{n3}^{j_{\text{eff}}} \\
&= \frac{2}{3\lambda_{\text{SO}}} \left[ \sum_{n=5}^8 \underbrace{\mathcal{H}_{1n}^{j_{\text{eff}}} \mathcal{H}_{n3}^{j_{\text{eff}}}}_{=0} + \sum_{n=9}^{12} \mathcal{H}_{1n}^{j_{\text{eff}}} \underbrace{\mathcal{H}_{n3}^{j_{\text{eff}}}}_{=0} \right] = 0 \\
\Rightarrow \Delta\mathcal{H}_{13}^{j_{\text{eff}}} &= \Delta\mathcal{H}_{14}^{j_{\text{eff}}} = \Delta\mathcal{H}_{23}^{j_{\text{eff}}} = \Delta\mathcal{H}_{24}^{j_{\text{eff}}} = \Delta\mathcal{H}_{31}^{j_{\text{eff}}} = \Delta\mathcal{H}_{41}^{j_{\text{eff}}} = \Delta\mathcal{H}_{32}^{j_{\text{eff}}} = \Delta\mathcal{H}_{42}^{j_{\text{eff}}} = 0.
\end{aligned}$$

Since the second-order corrections to the hopping elements in the  $j_{\text{eff}} = 1/2$  block vanish, the mixing between  $j_{\text{eff}} = 1/2$  and  $3/2$  blocks through the hopping terms are suppressed in these lacunar spinel compounds. Consequently, the effective Hamiltonian for the lacunar spinel compounds can be written as

$$\mathcal{H}_{\text{eff}} \simeq \mathcal{H}^{1/2} \oplus \mathcal{H}^{3/2}. \quad (10)$$

## Supplementary Note 4: DFT+SOC+ $U$ Results

*4.A. Calculation Details.* In this subsection, we explain the choice of initial magnetic configurations and the range of  $U_{\text{eff}}$  values we used in DFT+SOC+ $U$  calculations. Three different initial magnetic configurations within the  $M_4$  cluster — the all-in-all-out, the 2-in-2-out, and the collinear order, as shown in Supplementary Figure 3 (a), (b), and (c), respectively — are tried to detect the non-collinear order. For the magnetic order between the molecular moments on the neighboring  $M_4$  clusters, ferromagnetic (FM) and antiferromagnetic (AFM) orders are considered. A doubled unit cell with two formula units is used to incorporate the AFM order. In order to choose reasonable  $U_{\text{eff}}$  values, we referred to the work of Şaşıoğlu and co-workers, where the  $U$  and  $J$  values for transition metals are evaluated as functions of  $d$  orbital occupation from the constrained RPA calculations<sup>6</sup>;  $U_{\text{eff}}$  values are estimated around 1.0 ~ 2.0 eV for  $d^3$  and  $d^4$  configurations of  $4d$  and  $5d$  transition metal atoms. Taking account of the small  $d$  orbital occupations —  $d^{1.75}$  for  $M = \text{Nb}/\text{Ta}$  and  $d^{2.75}$  for  $\text{Mo}/\text{W}$  — and spatially extended molecular  $t_2$  orbitals, we suppose that the reasonable value of  $U_{\text{eff}}$  does not exceed 2.5 eV and 2.0 eV for the  $4d$  and  $5d$  compounds, respectively. Here, we use  $1.5 \leq U_{\text{eff}} \leq 2.5$  eV and  $1.0 \leq U_{\text{eff}} \leq 2.0$  eV for the  $4d$  and  $5d$  lacunar spinel compounds, respectively.

*4.B.  $j_{\text{eff}}$ -projected Bands and Density of States of FM Configuration.* Supplementary Figure 4 shows the  $j_{\text{eff}}$ -projected band structures and PDOS of  $\text{GaTa}_4\text{Se}_4\text{Te}_4$ ,  $\text{GaW}_4\text{Se}_4\text{Te}_4$ ,  $\text{GaNb}_4\text{Se}_8$ , and  $\text{GaMo}_4\text{Se}_8$  in FM order. The same  $U_{\text{eff}}$  values with the AFM calculations are used: 2.0 and 2.5 eV for  $5d$  and  $4d$  compounds, respectively. In common with the AFM results shown in Fig. 3 in the main text, the gap opening and the robust  $j_{\text{eff}}$  character are seen in the low-energy spectrum of all the compounds. The magnetic moments on the four corners of the  $M_4$  cluster are collinear for  $M = \text{Ta}, \text{W}, \text{Mo}$  compounds, while in  $\text{GaNb}_4\text{Se}_8$  a non-collinear order develops.

*4.C. Molecular  $t_2$  Character and Collinearity within  $M_4$  Cluster.* Once the low-energy electronic degrees of freedom are perfectly characterized by the molecular  $t_2$  states, the angular momenta at the four corners of the  $M_4$  cluster should be collinear. This is purely owing to the nature of the molecular  $t_2$  states, where their orbital components are identical at each transition metal site. More specifically, any wavefunction written as a linear combination of

the molecular  $t_2$  states reads

$$\begin{aligned}
 |\psi\rangle &= \sum_{\alpha=1}^3 \sum_{\sigma=\uparrow\downarrow} c_{\alpha}^{\sigma} |s_z = \sigma\rangle |D_{\alpha}\rangle \\
 &= \frac{1}{2} \sum_{i=1}^4 \left( \sum_{\alpha=1}^3 \sum_{\sigma=\uparrow\downarrow} c_{\alpha}^{\sigma} |s_z = \sigma\rangle |d_{\alpha}^i\rangle \right), \tag{11}
 \end{aligned}$$

where  $i = 1, \dots, 4$  are the  $M_4$  corner index, and  $\alpha$  denotes the orbital index  $xy, yz, xz$ . Regardless of the site index  $i$ , spin and orbital components in Eq. (7) are the same; in other words, the coefficient  $c_{\alpha}^{\sigma}$  does not have the site index  $i$ . The implication of this result is simple; as long as the molecular  $t_2$  states are perfectly isolated near the Fermi level, magnetic moments at the four corners of the  $M_4$  cluster are collinear and behave as a single moment. The only way to introduce non-collinear order is to make a mixture of molecular  $t_2$  states with other molecular states.

*4.D. Magnetic Order in DFT+SOC+U Calculations.* In this subsection, we discuss the magnetic order from the DFT+SOC+U calculations and their  $U_{\text{eff}}$  dependence. Detailed results — spin/orbital moments within the  $M_4$  cluster, and the relative energy between the FM and AFM configurations — are tabulated in Supplementary Table 2-5.

For the  $j_{\text{eff}} = 1/2$  compounds ( $M = \text{Mo}, \text{W}$ ), collinear orders within the  $M_4$  cluster are observed both in the FM and AFM states in the whole range of  $U_{\text{eff}}$  values we considered. Supplementary Figure 5 (a) and (b) show the magnetic moments of  $\text{GaW}_4\text{Se}_4\text{Te}_4$  and  $\text{GaMo}_4\text{Se}_8$  in the FM configuration at  $U_{\text{eff}} = 2.0$  and  $2.5$  eV, respectively. Spin and orbital angular momentum (SAM and OAM) align parallel to each other owing to the  $j_{\text{eff}} = 1/2$  character. The total sum of each moment within the  $M_4$  cluster is quite close to the ideal  $j_{\text{eff}} = 1/2$  moment ( $1/6$  and  $2/3 \mu_B$  for SAM and OAM, respectively) with small  $U_{\text{eff}}$  dependence. These reflect the nature of the pure  $j_{\text{eff}} = 1/2$  character of the unoccupied upper Hubbard bands in these compounds. The AFM and the FM states are nearly degenerate; the energy difference is smaller than  $0.3$  meV for  $U_{\text{eff}} \geq 1.5$  eV. This might imply the competing anisotropic exchange interactions with Heisenberg terms as mentioned in the main text, which needs more elaborate investigations on magnetism.

For  $\text{GaTa}_4\text{Se}_4\text{Te}_4$ , the system changes from a paramagnetic metal to a magnetic insulator in between  $U_{\text{eff}} = 1.0$  and  $1.5$  eV. Supplementary Figure 5 (c) shows the magnetic moments of  $\text{GaTa}_4\text{Se}_4\text{Te}_4$  in the FM configuration at  $U_{\text{eff}} = 2.0$  eV, where the large OAM with collinear

order dominates over the small canted SAM. SAM and OAM at each of the  $M_4$  corners tend to align antiparallel to each other owing to the  $j_{\text{eff}} = 3/2$  character. Contrary to the  $j_{\text{eff}} = 1/2$  systems, the FM configuration becomes more stable than AFM by 6.5 meV per formula unit at  $U_{\text{eff}} = 2.0$  eV.

In  $\text{GaNb}_4\text{Se}_8$ , the system turns from a paramagnetic metal to a non-collinear ordered insulator for  $U_{\text{eff}} \geq 2.0$  eV; Supplementary Figure 5 (d) shows the magnetic order at  $U_{\text{eff}} = 2.5$  eV in the FM calculation. Such non-collinear orders can be attributed to the mixing between the molecular  $t_2$  and the molecular  $e$  states, which is shown in Supplementary Figure 6 depicting the PDOS of  $\text{GaNb}_4\text{Se}_8$  at  $U_{\text{eff}} = 2.5$  eV. The AFM calculations, which are energetically more stable than FM results, show different non-collinear ordering compared to the FM results. From these results, one can say that  $\text{GaNb}_4\text{Se}_8$  shows weaker molecular  $t_2$  and  $j_{\text{eff}}$  character compared to the other compounds in the presence of large electron correlations. Still, the molecular  $j_{\text{eff}} = 3/2$  character prevails in the low-energy spectrum of  $\text{GaNb}_4\text{Se}_8$  as shown in Supplementary Figure 6. The competition between the electron correlations and the molecular nature as well as the atomic SOC may induce complicated internal structures of SAM and OAM within the  $M_4$  cluster, which calls for further studies.

**Supplementary Note 5:  $j_{\text{eff}} = 1/2$  Spin Hamiltonian.** The detailed expression for the  $j_{\text{eff}} = 1/2$  spin Hamiltonian in the strong coupling regime is as follows<sup>7</sup>:

$$\mathcal{H}_{\text{spin}}^{1/2} = \sum_{\langle ij \rangle} [J\mathbf{s}_i \cdot \mathbf{s}_j + \mathbf{D}_{ij} \cdot (\mathbf{s}_i \times \mathbf{s}_j) + \mathbf{s}_i \cdot \mathbf{A}_{ij} \cdot \mathbf{s}_j] \quad (12)$$

with

$$J = \frac{4}{U}t_0^2$$

$$\mathbf{D}_{ij} = \frac{4}{U}t_0 (\mathbf{t}_{ij}^{\text{D}} - \mathbf{t}_{ji}^{\text{D}})$$

$$\mathbf{A}_{ij} = -\frac{4}{U} (\mathbf{t}_{ji}^{\text{D}} \otimes \mathbf{t}_{ij}^{\text{D}} + \mathbf{t}_{ij}^{\text{D}} \otimes \mathbf{t}_{ji}^{\text{D}} - \mathbf{t}_{ij}^{\text{D}} \cdot \mathbf{t}_{ji}^{\text{D}})$$

where  $\otimes$  denotes the outer product of two vectors. Note that the Dzyaloshinskii-Moriya vector  $\mathbf{D}_{ij}$  is proportional to  $\mathbf{t}_{ij}^{\text{D}}$  since  $\mathbf{t}_{ij}^{\text{D}} = -\mathbf{t}_{ji}^{\text{D}}$ .

## Supplementary References

- <sup>1</sup> C. H. Kim, H.-S. Kim, H. Jeong, H. Jin, and J. Yu, Topological quantum phase transition in  $5d$  transition metal oxide  $\text{Na}_2\text{IrO}_3$ , *Physical Review Letters* **108**, 106401 (2012).
- <sup>2</sup> H.-S. Kim, C. H. Kim, H. Jeong, H. Jin, and J. Yu, Strain-induced topological insulator phase and effective magnetic interactions in  $\text{Li}_2\text{IrO}_3$ , *Physical Review B* **87**, 165117 (2013).
- <sup>3</sup> A. Camjayi, R. Weht, and M. Rozenberg, Localised Wannier orbital basis for the Mott insulators  $\text{GaV}_4\text{S}_8$  and  $\text{GaTa}_4\text{Se}_8$ , *Europhysics Letters* **100**, 57004 (2012).
- <sup>4</sup> B. J. Kim, H. Jin, S. J. Moon, J. Y. Kim, B. G. Park, C. S. Leem, J. Yu, T. W. Noh, C. Kim, S. J. Oh, J. H. Park, V. Durairaj, G. Cao, and E. Rotenberg, Novel  $J_{\text{eff}}=1/2$  Mott state induced by relativistic spin-orbit coupling in  $\text{Sr}_2\text{IrO}_4$ , *Physical Review Letters* **101**, 076402 (2008).
- <sup>5</sup> S. Murakami, N. Nagaosa, and S.-C. Zhang,  $\text{SU}(2)$  non-Abelian holonomy and dissipationless spin current in semiconductors, *Physical Review B* **69**, 235206 (2004).
- <sup>6</sup> E. Şaşıoğlu, C. Friedrich, and S. Blügel, Effective Coulomb interaction in transition metals from constrained random-phase approximation, *Physical Review B* **83**, 121101(R) (2011).
- <sup>7</sup> T. Micklitz and M. R. Norman, Spin Hamiltonian of hyper-kagome  $\text{Na}_4\text{Ir}_3\text{O}_8$ , *Physical Review B* **81**, 174417 (2010).